Optimization of Photovoltaic and Wind Generation Systems for Autonomous Microgrids With PEV-Parking Lots

Abdelfatah Ali, Karar Mahmoud, and Matti Lehtonen

***Abstract*—Lately, the integration of renewable energy sources (e.g., photovoltaic and wind generation systems) has been raised into microgrids interconnected with plug-in electric vehicles (PEVs). Such intermittent generation and charging/discharging PEV profiles are challenging to ensure the secure and optimal operation of microgrids. In this article, an optimization approach is proposed to determine the optimal locations and sizes of photovoltaic and wind generation systems in microgrids with PEV-parking lots. The developed approach addresses 1) the uncertainty of generation profiles of photovoltaic and wind generation systems and loads; 2) the DSTATCOM feature of photovoltaic and wind generation systems; and 3) microgrid constraints. The feasible PEV conditions are also considered, i.e., initial and preset conditions of their state of charge, arriving and departing times, and various controlled/uncontrolled charging schemes. To solve the planning model, we have developed a bilevel metaheuristic-based approach. The upper-level and lower-level optimization tasks are to optimize the decision variables of renewable energy sources and PEVs, respectively. Both energy losses through the lines and energy from the main grid are considered as subobjectives to be minimized. Various simulations and study cases are performed to assess the effectiveness of the proposed approach. The outcomes show the efficacy of the proposed approach to simultaneously plan renewable energy sources and manage PEVs to form an autonomous microgrid.**

***Index Terms*—Electric vehicles, energy losses, microgrid, photovoltaic, wind generation.**

I. Introduction

THE penetration of renewable energy sources (RESs) is increasing year by year globally. This trend is driven by global strategies to reduce greenhouse gas emissions, whereas breakthroughs are needed with respect to the future arrangements of electrical power productions. It is a fact that photovoltaic (PV) and wind turbine (WT) are the most notable alternatives of RESs due to their flexibility and cost-effectiveness [1]–[3]. Interestingly, RESs could lead to distinct constructive influences on the performance of distribution systems. In particular, with their smart functions, PV and WT units can raise the reliability of the supply, solve voltage violation issues, enhance power quality, minimize energy losses, and mitigate the burden on the conventional regulating components [4]–[6]. Though, the highly intermittent generation of PV and WT units can lead to extensive practical and operational issues, and so restraining their permitted accommodating capacities in distribution systems.

In concurrence with the increasing pattern of PV and WT, the interest in plug-in electric vehicles (PEVs) has extensively been expanding internationally [7]–[9], where their number has reached 20 million in 2020 [10]. Gathering several PEVs in PEV-parking lots can provide the distribution system operator with the opportunity of the batteries of PEVs, which can be employed as potential storage. From the grid perspective, the batteries of existing PEVs in parking lots can be charged or discharged while considering their preset charging goal according to the departing time [11]–[13]. Aggregators can control the energy storage ability of PEVs during parking time, where their average parking duration is more than 90% of the day [14], [15]. However, the stochastic nature of PEVs with their various charging schemes can cause several operational problems in the distribution systems. The most common problems are voltage violations, high losses, and line congestions, especially in the case of employing uncontrolled charging schemes of PEV batteries [16].

There is a growing literature aimed at optimizing the locations and the sizes of RESs to improve distinct performance indexes in distribution systems. Atwa *et al.* [17] introduced a probabilistic model for planning various RES types in distribution systems to maximizing energy loss reduction and satisfying system limits. Different analytical based methods are formulated in [18]–[20], which can calculate the optimal locations and sites of PV and WT units by considering the nominal load/generation conditions, and so missing the sufficient representation of the intermittent profiles. Kumar and Tyagi [21] proposed a cost-based optimization model utilizing stochastic programming for obtaining the optimal capacity of distributed energy resources. In [22], two iterative search-based methods have been introduced for determining the optimal capacities of WT, PV, and the battery energy

Manuscript received December 17, 2020; revised April 8, 2021; accepted July 12, 2021. Date of publication August 13, 2021; date of current version June 13, 2022. This work was supported by the Department of Electrical Engineering and Automation, Aalto University, Finland. *(Corresponding author: Karar Mahmoud.)*

Abdelfatah Ali is with the Faculty of Engineering, South Valley University, Qena 83523, Egypt (e-mail: engaaa2010@gmail.com).

Karar Mahmoud is with the Department of Electrical Engineering and Automation, Aalto University, FI-00076 Espoo, Finland, and also with the Faculty of Engineering, Aswan University, Aswan 81542, Egypt (e-mail: karar.alnagar@aswu.edu.eg).

Matti Lehtonen is with the Department of Electrical Engineering and Automation, Aalto University, FI-00076 Espoo, Finland (e-mail: matti.lehtonen@aalto.fi).

Digital Object Identifier 10.1109/JSYST.2021.3097256

This work is licensed under a Creative Commons Attribution 4.0 License. For more information, see https://creativecommons.org/licenses/by/4.0/

storage system in a microgrid. An optimization framework has been proposed in [23] for managing and sizing battery, PEV, and PV in smart homes. Vahidinasab [24] introduced a multiobjective framework that aims to optimally plan PV and WT units considering their probabilistic models in distribution systems while optimizing costs as well as carbon emissions. The hosting capacity of PV and WT has been improved by utilizing coordinated control scheme and reactive power support in [25] and [26]. Due to the current revolutions in creating and developing efficient metaheuristic optimization solvers, diverse types have been employed for RES planning in distribution systems, especially for multiobjective frameworks. Common examples are: crow search algorithm autodrive particle swarm optimization solver [27], tabu search optimization solver [28], genetic-based optimization solver [29], artificial ecosystem-based optimization [30], simulated annealing optimization solver [31], and ant colony optimization solver [32]. Regarding energy storage systems and PEVs, their vital contribution to growing the RES hosting capacity has been explored in [33]. Seddig *et al.* [34] developed control schemes of PEV batteries to raise the RES capacity in distribution systems.

Based on the aforementioned literature review, diverse approaches have been introduced for the optimal planning of PV and/or WT units in distribution systems. Yet, to lessen the computational burden of the optimization paradigm, some present methods adopt one RES unit planning with considering only active power generation and formulate deterministic rather than probabilistic planning models. Another vital demerit of many other approaches is missing the full representation of PEV batteries with their intermittent and uncertain charging and discharging profiles. It is a fact that the influence of such flexible PEVs is significant in distribution systems, which also can have considerable impacts on the RES planning problem. Hence, inclusive modeling of PEVs is compulsory while incorporating their charging schemes and stochastic variables and settings in the planning stage of RESs. To cover this research gap, this article is focused on such important research issues, whereas more studies and advances are essential, considering PV units, WT units, and PEVs.

In this article, we have proposed a new bilevel optimization-based approach for optimally locating and sizing both PV and WT units in microgrids considering PEV-parking lots. The main advantages of the proposed approach include considering the following: 1) the intermittent profiles of PV and WT generation; and loads; 2) the DSTATCOM functionalities of PV and WT inverters; and 3) various constraints of the microgrid. Another vital contribution is incorporating the practical PEV variables and parameters in the planning model, including arriving and departing times, initial and preset conditions of their state of charge (SOC), and different controlled /uncontrolled charging schemes. The proposed bilevel metaheuristic-based approach is used to accurately solve this comprehensive planning model. Specifically, its upper-level and lower-level optimization duties are to optimally compute the decision variables of RESs and PEVs, respectively. Regarding the objective function, we have assigned the energy losses through the lines as well as the energy from the main grid to be minimized. To demonstrate the effectiveness of the proposed approach, various simulations and study cases are performed on the IEEE 69-bus distribution system. The efficacy of the proposed approach is proved to simultaneously plan renewable energy sources and manage PEV batteries while contributing to the transformation towards autonomous microgrids.

II. Problem Formulation

In this section, we describe the planning model for optimizing PV and wind generation systems in grid-connected microgrid interconnected with PEV-parking lots. Since the tie-line power between the utility power grid and microgrid may have high fluctuations due to the integration of PV and wind turbines in the microgrid, these fluctuations can lead to numerous technical problems such as voltage fluctuations and excessive power losses. Therefore, the tie-line power and energy losses are utilized as subobjectives to be minimized in the planning problem. Moreover, minimizing the tie-line power makes the microgrid near to be autonomous. The objective function and constraints of the optimization model can be expressed as follows.

A. Objective Function

$$\text{Minimize}\,\{\text{Objective 1}, \text{Objective 2}\} \tag{1}$$

where Objective 1 and Objective 2 are the active power losses and the tie-line power, respectively, and can be described as follows.

1) Active Power Losses:

$$\text{Objective 1} = \sum_{t=1}^{n_t}\sum_{s=1}^{n_s} P^t_{\text{Loss},s} \times CP \tag{2}$$

in which

$$P_{\text{Loss}} = \sum_{\text{i}=1}^{N_{\text{L}}} G_{ij}(V_i^2(\text{tap}_{ij,s})^2 + V_j^2 - 2V_iV_j\text{tap}_{ij,s}\cos\delta_{ij}) \tag{3}$$

where $P^t_{\text{Loss},s}$is the active power losses in the microgrid at time instant t for state *s*; n_t and n_s are the number of time instants and number of states; CP represents the combined probability of solar irradiance, wind speed, and load demand; N_L is the number of the lines; G_{ij} represents the conductance of the line between buses *i* and *j*. $\text{tap}_{ij,s}$ represents the tap position of the OLTC of the line between buses *i* and *j*.

2) Tie-Line Power:

$$\text{Objective 2} = \sum_{t=1}^{n_t}\sum_{s=1}^{n_s} P^t_{\text{Tie-line},s} \times CP \tag{4}$$

where $P^t_{\text{Tie-line},s}$ represents the tie-line power between the utility grid and microgrid.

B. Constraints

$$n_iP^t_{\text{WT},i,s} + P^t_{\text{PV},i,s} - P^t_{d,i,s} \pm P^t_{PL,i,s} - V^t_{i,s}\sum_{j=1}^{n_b} V^t_{j,s}ta\text{p}_{ij,s}\begin{bmatrix} G_{ij}\cos\delta^t_{ij,s} \\ +B_{ij}\sin\delta^t_{ij,s}\end{bmatrix} = 0 \tag{5}$$

$$Q^t_{\text{inv,PV},i,s} + Q^t_{\text{inv,WT},i,s} - Q^t_{d,i,s} - V^t_{i,s}\sum_{j=1}^{n_b} V^t_{j,s}\text{tap}_{ij,s}$$

$$\times \begin{bmatrix} G_{ij}\sin\delta^t_{ij,s} \\ +B_{ij}\cos\delta^t_{ij,s} \end{bmatrix} = 0, \quad \forall i \notin \phi_b, s, t \tag{6}$$

$$V^{\min} \le V^t_{i,s} \le V^{\max}, \quad \forall i \in \phi_b, s, t \tag{7}$$

$$P^{\min,t}_{\mathrm{PL},i,s} \le P^t_{PL,i,s} \le P^{\max,t}_{\mathrm{PL},i,s}, \quad \forall i \in \phi_b, s, t \tag{8}$$

$$n^{\min}_i \le n_i \le n^{\max}_i, \quad \forall i \in \phi_b \tag{9}$$

$$C^{\min}_{\mathrm{PV},i} \le C_{\mathrm{PV},i} \le C^{\max}_{\mathrm{PV},i}, \quad \forall i \in \phi_b \tag{10}$$

$$C^{\min}_{\mathrm{WT},i} \le C_{\mathrm{WT},i} \le C^{\max}_{\mathrm{WT},i}, \quad \forall i \in \phi_b \tag{11}$$

$$\sum_{i=1}^{N_{\mathrm{PV}}} P_{\mathrm{PV},i} \le R^{\max}_{\mathrm{PV}} \tag{12}$$

$$\sum_{i=1}^{N_{\mathrm{WT}}} P_{\mathrm{WT},i} \le R^{\max}_{\mathrm{WT}} \tag{13}$$

$$Q^{\min,t}_{\mathrm{inv,PV},i,s} \le Q^t_{\mathrm{inv,PV},i,s} \le Q^{\max,t}_{\mathrm{inv,PV},i,s}, \quad \forall i \in \phi_b, s, t \tag{14}$$

$$Q^{\min,t}_{\mathrm{inv,WT},i,s} \le Q^t_{\mathrm{inv,WT},i,s} \le Q^{\max,t}_{\mathrm{inv,WT},i,s}, \ \forall i \in \phi_b, s, t \tag{15}$$

$$\begin{cases} Q^{\max,t}_{\mathrm{inv,PV},i,s} = \sqrt{S^2_{\mathrm{inv,PV},i} - \left(P^t_{\mathrm{PV},i,s}\right)^2} \\ Q^{\min,t}_{\mathrm{inv,PV},i,s} = -\sqrt{S^2_{\mathrm{inv,PV},i} - \left(P^t_{\mathrm{PV},i,s}\right)^2} \end{cases} \tag{16}$$

$$\begin{cases} Q^{\max,t}_{\mathrm{inv,WT},i,s} = \sqrt{S^2_{\mathrm{inv,WT},i} - \left(P^t_{\mathrm{WT},i,s}\right)^2} \\ Q^{\min,t}_{\mathrm{inv,WT},i,s} = -\sqrt{S^2_{\mathrm{inv,WT},i} - \left(P^t_{\mathrm{WT},i,s}\right)^2} \end{cases} \tag{17}$$

$$\mathrm{tap}^{\min} \le \mathrm{tap}^t_{ij} \le \mathrm{tap}^{\max} \forall (i,j) \in \varphi_r \tag{18}$$

$$\mathrm{SOC}_{n,d,s} \ge \mathrm{SOC}_{n,\min,s} \tag{19}$$

where B_{ij} is the susceptance of the line between buses *i* and *j;* $V^t_{i,s}$ the voltage magnitude at *i*th node; $\delta^t_{ij,s}$is the voltage angle variance at *i*th and *j*th buses; $P^t_{d,i}$ and $P^t_{\mathrm{PL},j,s}$are, respectively, the load demand and parking lot power; $P^t_{\mathrm{WT},i,s}$ is the generated power of the wind turbine at bus *i*; $P^t_{\mathrm{PV},i,s}$ is the generated power of the PV unit at bus *i*; n_b is the number of nodes; $Q^t_{d,i}$is the reactive power demand; n_i is the allowed number of wind turbines at bus *i;* $C_{\mathrm{PV},i}$ and $C_{\mathrm{WT},i}$ are the capacities of PV and WT units, respectively; $R^{\max}_{\mathrm{PV}}$ and $R^{\max}_{\mathrm{WT}}$ are the maximum total PV size and maximum total WT size, respectively*;* $S_{\mathrm{inv,PV},i}$ is the rating of the interfacing inverter of PV; $Q^t_{\mathrm{inv,PV},i,s}$ represents the reactive power of the interfacing inverter of PV at *i*th node; $S_{\mathrm{inv,WT},i}$ is the rating of the interfacing inverter of WT; $Q^t_{\mathrm{inv,WT},i,s}$represents the reactive power of the interfacing inverter of wind turbines at *i*th node. Note that the main focus of this article is the planning phase of PV and WT units, not their operational phase. For this reason, we treat the reactive power in the steady-state condition, which is a widely procedure in the literature. ϕ_b represents a set of the system buses; φ_r represents a set of the system branches; $\mathrm{SOC}_{n,d,s}$ represents the SOC of *n*th battery at parting time; $\mathrm{SOC}_{n,\min,s}$ is the minimum SOC determined by the vehicle owner; the superscripts $\min$ and $\max$ represent the minimum and maximum limits of the control and the dependent variables, respectively. In this article, we have not considered the specifications of DSTATCOM feature of PV and inverter topology. However, we have considered the effect of the reactive power, which can be injected/absorbed by the interfacing inverters at the PV terminal on the microgrid.

C. Modeling of PEV Battery

The SOC is the main characteristic of the PEV battery. The SOC of the PEV battery can be increased or decreased based on the charging/discharging power. Hence, the SOC can be updated at each time instant as follows:

$$\mathrm{SOC}^t_{n,s} = \mathrm{SOC}^{t-1}_{n,s} + \eta_{ch,n} P^t_{ch,n,s} \Delta t \delta - \frac{\Delta t \gamma P^t_{\mathrm{dc},n,s}}{\eta_{\mathrm{dc},n}} \tag{20}$$

where $P^t_{ch,n,s}$is the charging power of *n*th PEV battery at time segment *t* for state *s*; $P^t_{\mathrm{dc},n,s}$ is the discharging power of *n*th PEV battery at time segment *t* for state *s*; δ and γ belong to {01}; it is worth mentioning that the PEV cannot charge and discharge at the same time, therefore, $\delta.\gamma = 0$; $\eta_{ch,n}$ represents the charging efficiency while $\eta_{\mathrm{dc},n}$ represents the efficiency of the discharging of the *n*th PEV.

Each PEV has a part of the total charging/discharging power of the parking lot. The charging/discharging power of each PEV depends on many factors such as 1) battery capacity of the PEV($C_{\mathrm{batt},n}$); 2) the current SOC of the PEV($\mathrm{SOC}^t_{n,s}$); 3) the arriving time of the PEV(T_{arr}); and 4) the time of the parting($T_{d,n}$). Therefore, the charging/discharging power of a PEV can be computed as follows:

$$P^t_{ch,n,s} = \frac{\left(C_{\mathrm{batt},n} - \mathrm{SOC}^t_{n,s} \times C_{\mathrm{batt},n}\right) \times P^t_{\mathrm{PL},s}}{T_{\mathrm{rem},n} \times \sum_{j=1}^{m} \frac{1}{T_{\mathrm{rem},j}} \left(C_{\mathrm{batt},j} - \mathrm{SOC}^t_{j,s} \times C_{\mathrm{batt},j}\right)} \tag{21}$$

$$P^t_{\mathrm{dc},n,s} = \frac{T_{\mathrm{rem},n}\left(\mathrm{SOC}^t_{n,s} \times C_{\mathrm{batt},n}\right) \times P^t_{\mathrm{PL},s}}{\sum_{j=1}^{m} T_{\mathrm{rem},j}\left(\mathrm{SOC}^t_{j,s} \times C_{\mathrm{batt},j}\right)} \tag{22}$$

$$T_{\mathrm{rem},n} = T_{d,n} - T_{arr,n}. \tag{23}$$

D. Stochastic Behavior of PEV

There are many stochastic variables in the PEVs profiles, such as 1) daily traveling milage; 2) the arrival time to the parking lot; 3) paring time; 4) driving habits; 5) the capacity of the connected PEV; and 6) the charging and discharging efficiencies of the PEV. These stochastic variables are the key characteristics that can describe PEV owners' performance and preferences. Therefore, we have to consider these variables in the planning problem. For each PEV, the arrival time is a random variable described by a normal probability density function (pdf) [35]. Hence, the daily arrival time of a PEV can be given by

$$f^t_n\left(T_{arr}\right) = \exp\left[\frac{-\left(T_{arr} - \mu^t_{T_{arr}}\right)^2}{2\left(\sigma^t_{T_{arr}}\right)^2}\right] \Big/ \left(\sigma^t_{T_{arr}}\sqrt{2\pi}\right) \tag{24}$$

where $\mu^t_{T_{arr}}$ and $\sigma^t_{T_{arr}}$ represent, respectively, the mean of daily arrival time, and it is 18 h and a standard deviation of daily arrival time, and it is 5 h.

The initial SOC of each PEV varies based on 1) daily traveling mileage (dm_n); 2) SOC at the last departure time (assumed to be 100%); and 3) all-electric range (AER_n). The depth of discharge should not be more than 80% for protecting the PEV against degradation. Therefore, the initial SOC of a PEV can be determined by the following formula:

$$\mathrm{SOC}_{\mathrm{initial},n}(\%) = \begin{cases} (1 - dm_n/\mathrm{AER}_n) \times 100, & 0 < dm_n < 0.8\mathrm{AER}_n \\ 20\%, & dm_n > 0.8\mathrm{AER}_n \end{cases} \tag{25}$$

$$\mathrm{AER} = C_{\mathrm{batt},n}/E_{\mathrm{cons/mile},n} \tag{26}$$

where $E_{\mathrm{cons/mile},n}$ represents the consumption energy per mile. The unpredictability of the daily traveling mileage for a PEV can be characterized by a lognormal pdf [35]. The pdf can be described as follow:

$$f^t_n(dm) = \frac{1}{dm_n\sqrt{2\pi(\sigma^t_{dm,n})^2}} \times \exp\left[\frac{-(\ln dm_n - \mu^t_{dm,n})^2}{2(\sigma^t_{dm,n})^2}\right],\ dm_n > 0 \tag{27}$$

where μ^t_{dm} is the mean of daily mileage, and it is 22.3; σ^t_{dm} is the standard deviation, and it is 12.3 miles.

III. Modeling of the Uncertainty

Here, the hourly uncertainty modeling of the wind generation system, PV generation system, and load demand are explained. Weibull pdf, Beta pdf, and normal pdf are employed, respectively, to model hourly uncertainty of wind speed, solar irradiance, and load demand [36], [37]. The probabilistic models can be described as follows.

A) Probabilistic Model of Wind Generation System

The generated power of the WT depends on the wind speed and the characteristics of the turbines themselves. Weibull pdf with shape parameter equal 2 is regularly utilized to model the wind speed [17], and it is called Rayleigh pdf [38]. Therefore, in this article, the data of hourly wind speed are used to generate the Rayleigh pdfs ($f^t_r(v)$) for each time segment (t), which can be described as follows:

$$f^t_r(v) = \left(\frac{2v}{c^2}\right)\exp\left[-\left(\frac{v}{c}\right)^2\right] \tag{28}$$

where v is the wind speed; c represents the Rayleigh scale parameter, and it can be computed by utilizing the historical data for each time segment. The continuous pdfs are divided into numerous portions in which each portion generates a mean value and a probability of occurrence. Therefore, the probability of each portion during any time segment (t) can be described as follows:

$$\mathrm{prob}^t_{v,i} = \int_{v_{w1}}^{v_{w2}} f^t_r(v)\,.dv_i \tag{29}$$

where v_{w1} and v_{w2} are the wind speed limits of the portion (state) i; $\mathrm{prob}^t_{v,i}$is the probability occurrence of state i for time segment t. Based on the characteristics of the WT unit, the wind speed of each state (w) is converted into the output power of the wind generation system ($P^t_{\mathrm{WT}_w}$) as follows:

$$P^t_{\mathrm{WT}_w} = \begin{cases} 0, & 0 \le v_{av,w,t} < v_{ci} \\ P_{\mathrm{rated}} \times \frac{(v_{av,w,t} - v_{ci})}{(v_r - v_{ci})}), & v_{ci} \le v_{av,w,t} < v_r \\ P_{\mathrm{rated}}, & v_r \le v_{av,w,t} < v_{co} \\ 0, & v_{av,w,t} \ge v_{co} \end{cases} \tag{30}$$

where the cut-in speed, cutoff speed, and rated speed are denoted by v_{ci}, v_{co}, and v_r, respectively; the average wind speed is indicated by $v_{av,w,t}$; the rated power of the WT is represented by P_{rated}.

B) Probabilistic Model of PV Generation System

The data of the solar irradiance each hour are employed to determine the Beta pdfs ($f^t_b(g_s)$) of the time segments and can be characterized as follows [36], [39]:

$$f^t_b(g_s) = \begin{cases} \frac{\Gamma(\alpha+\beta)}{\Gamma(\alpha).\Gamma(\beta)} g_s^{(\alpha-1)}.(1-g_s)^{(\beta-1)}, & 0 \le g_s \le 1;\ \alpha,\beta \ge 0 \\ 0, & \text{Otherwise} \end{cases} \tag{31}$$

in which

$$\beta = (1-\mu) \times \left(\frac{\mu \times (1+\mu)}{(\sigma)^2} - 1\right)$$

$$\alpha = \frac{\mu \times \beta}{1-\mu}.$$

Here, α and β are the Beta parameters for each time segment. These parameters can be computed by utilizing the mean (μ) and slandered deviation (σ), which are determined from the historical data [40], [41]. The continuous Beta pdfs are sliced into many portions where each portion generates a mean value and a probability of occurrence. The occurrence probability of a portion during a specific time segment ($\mathrm{prob}^t_{gs,i}$) can be computed by

$$\mathrm{prob}^t_{gs,i} = \int_{g_{s1}}^{g_{s2}} f_b(g_s)\,dg_{s,i} \tag{32}$$

where g_{s1} and g_{s2} are the limits of the solar irradiance of the portion i. The output power PV for each state (s) of time segment (t) ($P^t_{\mathrm{PV},s}$) can be calculated as follows:

$$P^t_{\mathrm{PV},s} = N \times \frac{V_{\mathrm{MPP}} \times I_{\mathrm{MPP}}}{V_{\mathrm{OC}} \times I_{\mathrm{SC}}} \times V^t_{\mathrm{cell},s} \times I^t_{\mathrm{cell},s} \tag{33}$$

$$I^t_{\mathrm{cell},s} = g_{s,t}\left(I_{\mathrm{SC}} + K_i\left(T^t_{\mathrm{cell},s} - 25\right)\right) \tag{34}$$

$$T^t_{\mathrm{cell},s} = T_A + g_{s,t}\left(\frac{N_{OT} - 20}{0.8}\right) \tag{35}$$

$$V^t_{\mathrm{cell},s} = V_{\mathrm{OC}} - K_v T^t_{\mathrm{cell},s} \tag{36}$$

where $T^t_{\mathrm{cell},s}$ represents the cell temperature; T_A represents the ambient temperature; NOT is the nominal operating temperature of the cell; N represents the number of PV modules; V_{MPP} and I_{MPP} represent, respectively, voltage and current at maximum

power point; $V^t_{\text{cell},s}$ and $I^t_{\text{cell},s}$ represent, respectively, cell voltage and cell current; K_v and K_i denote, respectively, the voltage and current temperature coefficients; I_{sc} and V_{oc} are the short circuit current and open-circuit voltage, respectively; $g_{s,t}$ is the solar irradiance; *t* and *s* represent the time instant and state, respectively.

C) Probabilistic Model of Load Demand

Due to the demand power uncertainty, a normal pdf is utilized for load modeling at each bus in the microgrid. The normal pdf of the load demand can be determined based on the following formula [41]:

$$f^t_N\ (l) = \frac{1}{\sigma_l\sqrt{2\pi}}\ \times \exp\left[-\left(\frac{l-\mu_l}{2\sigma_l^2}\right)\right] \tag{37}$$

where $f^t_N(l)$ is the normal pdf of the load demand; μ_l represents the mean of the load demand; σ_l represents the standard deviation of the load demand. The occurrence probability of a portion during a specific time instant $\text{prob}^t_{l,i}$ can be described as follows:

$$\text{prob}^t_{l,i} = \int_{l_1}^{l_2} f_N\,(l)\,dl \tag{38}$$

where l_1 and l_2 are the limits of the load demand in the interval *i*.

D) Combined Probabilistic Model of PV, Wind, and Load

The aforementioned probabilistic models of wind speed, solar irradiance, and load demand are employed to generate a combined probability model (CP) of wind-PV-load. The CP can be calculated by convolving the probabilities of the wind speed, solar irradiance, and load demand, as follows:

$$CP^t_i = \text{prob}^t_{v,i}\ \times \text{prob}^t_{gs,i} \times \text{prob}^t_{l,i}. \tag{39}$$

IV. Multiobjective Ant Lion Optimizer (MOALO)

MOALO was proposed in 2017 by Mirjalili *et al.* [42]. This algorithm mimics the hunting performance of antlions interacting with their favorite prey, ants, and them. The common actions of the Ant Lion Optimizer (ALO), which illustrate the interaction between antlions, the trapped ants are 1) random walk of ants; 2) traps building; 3) entrapment of trapped ants; 4) preys catching; and 5) rebuilding the traps and elitism. The ant lion builds a hole like a cone, where its edge is appropriately sharp for an ant at to fall to the bottom of it. The ant lion tries to catch the ant underneath the bottom of the cone. The MOALO can be mathematically modeled as follows.

Ants walk randomly in the search space, and their random work can be described by

$$X\ (\text{iter}) = [0,\ \text{cums}(2r(\text{iter}_1)\text{–}1), \ldots, \text{cums}(2r(\text{iter}_{\text{maxit}})\text{–}1)] \tag{40}$$

where cums computes the cumulative sum, maxit represents the maximum iteration number, iter denotes the step of random walk (number of iteration), and *r (*iter*)* represents the random function and can be described as follows:

$$r\ (\text{iter}) = \begin{cases} 1 \text{ if rand} > 0.5 \\ 0 \text{ if rand } \le 0.5 \end{cases} \tag{41}$$

where rand represents a random number generated in the range of [0,1].

To keep the random movements of the ants in the limits of the search space and prevent them from overshooting, the random movement of the ants should be normalized using the following expression:

$$X^{\text{iter}}_\chi = \frac{\left(X^{\text{iter}}_\chi - a_\chi\right) \times \left(d^{\text{iter}}_\chi - c^{\text{iter}}_\chi\right)}{\left(b_\chi - a_\chi\right)}\ + c^{\text{iter}}_\chi \tag{42}$$

where $c^{\text{iter}}_\chi$and d^{iter}_χ represent, respectively, the minimum and maximum of *x*th variable at iter[th] iteration; a_χ and b_χ are the minimum and maximum of random walk of *x*th variable at iter[th] iteration, respectively.

The trapping mechanism model of ant lions on the ants can be expressed as follows:

$$c^{\text{iter}}_\chi = \text{Antlion}^{\text{iter}}_h\ + c^{\text{iter}} \tag{43}$$

$$d^{\text{iter}}_\chi = \text{Antlion}^{\text{iter}}_h\ + d^{\text{iter}} \tag{44}$$

where c^{iter} and d^{iter} are, respectively, the minimum and maximum of all variables at iter[th] iteration; $\text{Antlion}^{\text{iter}}_h$ represents the position of the selected *h*th ant lion at the iter[th] iteration.

To simulate the sliding of the ants toward ant lions, the limits of random walks have to be decreased adaptively and can be described by

$$c^{\text{iter}} = \frac{c^{\text{iter}}}{I} \tag{45}$$

$$d^{\text{iter}} = \frac{d^{\text{iter}}}{I} \tag{46}$$

in which

$$I\ =\ 1 + 10^{\omega}\frac{\text{iter}}{\text{maxit}} \tag{47}$$

where ω is a constant, which is determined based on the current iteration. This parameter (ω) can regulate the accuracy level of exploitation.

The step before the last step of ALO is catching the ant rebuilding the new pits (updating the position of the selected ant lion). This can be mimicked by the following formula:

$$\text{Antlion}^{\text{iter}}_h + \text{Ant}^{\text{iter}}_\chi \text{ if f}\left(\text{Ant}^{\text{iter}}_\chi\right) < f\left(\text{Ant}^{\text{iter}}_\chi \text{Antlion}^{\text{iter}}_h\right) \tag{48}$$

where $\text{Ant}^{\text{iter}}_\chi$ represents the position of the χth ant at the iter[th] iteration.

The last step in the ALO is elitism, in which the best ant lion determined in every iteration is sored. This is the only ant lion that can affect the walks of all ants. Therefore, in the MOALO, all ants are considered to randomly move around the elite antlion, similar to moving around a selected antlion. This can be mathematically shown as follows:

$$\text{Ant}^{\text{iter}}_\chi = \frac{R^{\text{iter}}_E + R^{\text{iter}}_A}{2} \tag{49}$$

where R^{iter}_E denotes the random walk around the elite; and R^{iter}_A denotes the random walk around the selected ant lion. Note that the obtained solutions are global optimal ones since the developed ALO optimizer can avoid trapping in the local minima [42].

Pareto Optimal Solution: There is an efficient method for the multiobjective optimization problem called Pareto optimal approach. This method contains a cluster of dominant solutions

that make a compromise between objective functions. The Pareto optimal solutions can be depicted in a diagram called the Pareto diagram. For a multiobjective optimization problem, if X_1 and X_2 are solutions for the problem, then X_1 may be dominant or nondominant the solution X_2. In general, we can assume that X_1 dominate X_2 on if

$$\forall o \in \{12, \cdots, k\} : f_o(X_1) \leq f_o(X_2) \tag{50}$$

$$\exists o \in \{12, \cdots, k\} : f_o(X_1) < f_o(X_2) \tag{51}$$

where k is the number of control variables; o is the index of the objective function.

Best Compromise Solution: The nondominated solutions of MOALO in all iterations are saved in a repository. Hence, it is crucial to determine the best-compromised solution amongst these solutions. For this purpose, the fuzzy logic theory is utilized as a decision-maker [43]. The solution with the furthest distance from the worst solution and has the smallest distance from the ideal one is the best solution to the optimization problem. The worst and the best values of the objective function in a minimization problem are defined by $OF_o^{\min}$and $OF_o^{\max}$, respectively. The highest satisfaction and the lowest satisfaction are determined according to the membership (μ) value as follows:

$$\mu_o^k = \begin{cases} 1, & f_o \leq f_o^{\min} \\ \frac{f_o^{\max} - f_o}{f_o^{\max} - f_o^{\min}}, & f_o^{\min} \leq f_o \leq f_o^{\max} \\ 0, & f_o \geq f_o^{\max} \end{cases} \tag{52}$$

where 0 and 1 represent, respectively, the lowest and highest satisfactions; $f_o^{\min}$ and $f_o^{\max}$ are the minimum and maximum values of oth objective function; μ_o^k represents the membership value of kth nondominant solution for oth objective function. The best nondominant solution can be determined as follows:

$$\mu^k = \sum_{o=1}^{N_{obj}} \mu_o^k \Big/ \sum_{k=1}^{N_{nd}} \sum_{o=1}^{N_{obj}} \mu_o^k \tag{53}$$

where N_{obj} and N_{nd} represents, respectively, the number of objective functions and the number of nondominant solutions.

V. Solution Process

Here, we describe the solution process of the proposed planning approach for calculating the locations and sites of PV and WT units in distribution systems. The developed bilevel heuristic-based solution process is more suitable for the complex planning model the PV and WT units. Specifically, it involves three key stages: read data, run the proposed bilevel MOALO solver, and finally print planning results. In the first stage, it is required to read the full data of the distribution system under study, besides the parameters as well as historical datasets of load PV units and WT units to perform their combined probability model. Also, the operational limits of the distribution system, PV, WT, PEV units are monitored. Then, in the next stage, the proposed bilevel MOALO solver is employed to solve the planning model of RES. In particular, the bilevel MOALO solver involves two levels (lower-level and upper-level). The duties of upper-level and lower-level optimization are to optimally compute the decision variables of RES and PEVs, respectively. Algorithm 1 shows the solution procedure of the bilevel MOALO model for optimization of PV and WT systems considering PEVs in the microgrid.

Algorithm 1: Optimization of PV and Wind Generation Systems.

1: **Inputs:** Distribution system data, locations of PEV-parking lots, historical load, solar irradiance, and wind speed data.
2: **Outputs:** Locations and sizes of both PV and WT units.
3: Generate the combined probability model by utilizing (28)–(39).
4: Generate the probability model of daily arrival time and initial SOC of PEVs using (24)–(27).
5: **Procedure:** Bi-level MOALO
6: Setting the parameters of lower and upper levels.
7: Initializations of variables for lower and upper levels.
8: Calculate *Objective 1* and *Objective 2* for each search agent (ants and antlion) expressed by (1).
9: **While** ($iter1 < iter1_{max}$)
10: **For** each agent of the upper level **do**
11: Update the positions of the upper level using (40).
12: **end for**
13: Update the parameters of the lower level.
14: **While** ($iter2 < iter2_{max}$)
15: **For** each agent of the lower level **do**
16: Update positions of the lower level by (40).
17: **end for**
18: Update the parameters of the lower level.
19: Determine P_{PL} , Q_{inv}, and transformer tap position based on (8), (14)–(18).
20: Compute SOC, P_{ch}, and P_{dc} of EVs using (20)–(23).
21: Compute fitness of the lower layer using (3) and (4).
22: **End while**
23: Compute the BCS of lower level using (52) and (53).
24: Update the fitness of the upper layer using (1).
25: **End while**
26: Compute the BCS of upper level using (52) and (53).
27: **End Procedure**

Note that the lower-level must be wholly performed until reaching the stopping criteria for every iteration of the upper-level. This iterative solution process between the two levels is repeated till the stopping criteria of the upper-level is accomplished. Finally, the detailed calculated results of the planning problem are printed and saved. It is worth mentioning that the main contribution of PEV incorporation is to provide further benefits in terms of improving the objective functions through flexible charging and discharging abilities.

VI. Results and Discussions

A. Test System

In this article, the well-known 69-bus distribution system is used as a test system to evaluate the proposed approach. The system data (line and bus data) can be found in [44]. In our study, this system is divided into six different zones. Specifically, three

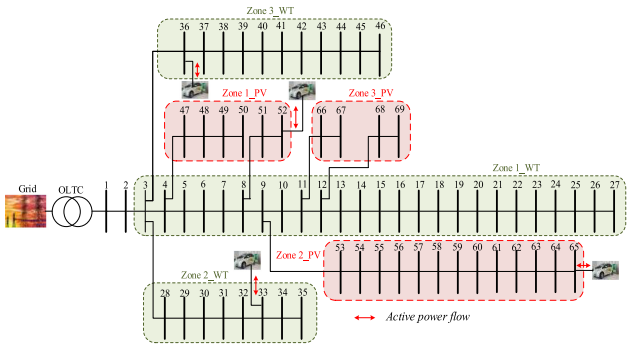

Fig. 1. Single line diagram of the 69-bus radial distribution system.

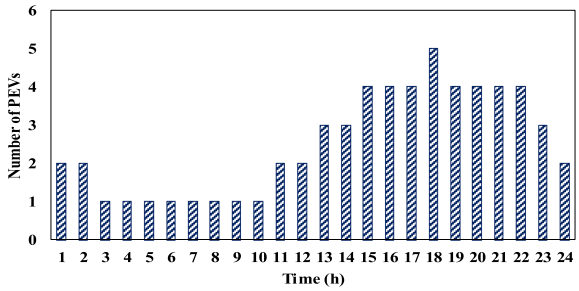

Fig. 2. Hourly distribution of 60 PEVs.

zones (Zone 1_PV, Zone 2_PV, and Zone 3_PV) are applicable for the PV allocation, and the other three zones (Zone 1_WT, Zone 2_WT, and Zone 3_WT) are appropriate for the WT allocation, as demonstrated in Fig. 1. Four parking lots for PEVs are assumed to be connected at buses 33, 36, 52, and 65, as shown in Fig. 1. Each parking lot can accommodate 60 PEVs. The distribution of the PEVs at each parking lot throughout is given in Fig. 2.

In this article, Tesla Model S batteries are employed for PEVs in which each battery has a capacity of 85 kWh [45]. Usually, the PEVs leave the parking lot in the morning (around 7:00) while they back home after working hours (around 18:00). Hence, each vehicle is expected to be plugged into the distribution system for 12 h. During the parking time of the PEVs, the option of vehicle-to-grid (V2G) technology can be employed, while enough SOC for each PEV at its parting time for daily mileages should be guaranteed. Here, the maximum charging and discharging rate of each PEV is 50% of the battery capacity ($0.5C_{\mathrm{batt},n}$) [8]. Two different types of DGs (PV and wind) are optimally allocated in the microgrid to minimize the annual energy losses and the tie-line power between the utility power grid and microgrid. In this article, it is assumed that DGs are utility-owned, and there are candidate zones for allocating PV units and other candidate zones for allocating WT units. The proposed approach is carried out without and with enabling the reactive power capability of the interfacing inverters of the RES. To demonstrate the effectiveness of the proposed approach, it is assessed for single and multiple combinations of PV and wind generation systems. The historical data of solar irradiance, wind speed, and load demand for three years are utilized to generate their probability. These data are gathered from [46], [47], and [48], respectively, where a day throughout these three years is used to represent them. The simulations are conducted on MATLAB.

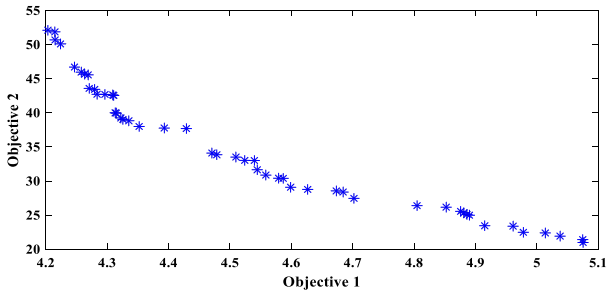

Fig. 3. Pareto-optimal solutions obtained for combined of one PV unit and one wind unit.

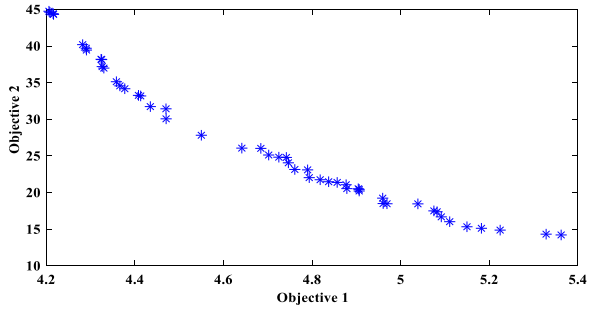

Fig. 4. Pareto-optimal solutions obtained for combined of two PV units and two wind units.

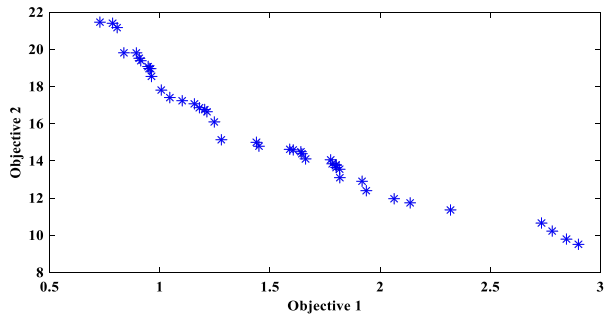

Fig. 5. Pareto-optimal solutions obtained for combined of three PV units and three wind units.

B. Performance Assessment of the Proposed Approach

To demonstrate the efficacy of the proposed approach, it is employed to allocate different combinations of PV and wind units in the grid-connected microgrid. The proposed approach allocates a mix of one PV unit and one wind unit, two PV units and two wind units, and three PV units and three wind units. It is worth mentioning that the ratio of these two renewable energy sources is considered as an input data by the system planner. In this article, we have considered these specified combinations of PV and WT units; However, any other combination can be solved by the developed approach.

Figs. 3, 4, and 5 show the set of dominant points (Objective 1 and Objective 2) for one PV unit and one wind unit, two PV units and two wind units, and three PV units and three wind units, respectively. The optimal locations and sizes obtained by the

TABLE I
OBTAINED SOLUTIONS FOR 69-BUS DISTRIBUTION SYSTEM

Item	Base Case	1 PV& 1WT	2PV& 2WT		3PV & 3WT		
PV locations	-	51	51	66	50	60	68
WT locations	-	12	18	28	11	31	41
PV sizes (MW)	-	2.87	1.23	1.69	0.95	1.37	0.14
WT sizes (MW)	-	2.92	0.69	2.73	1.09	1.91	1.41
Annual energy loss (MWh)	1856	1149	1179		426		
Annual energy loss reduction (%)	-	38.00	36.50		77.00		
Average tie-line power (MVA)	4.85	0.98	0.79		0.50		
Reduction of tie-line power (%)	-	80.00	84.00		90.00		

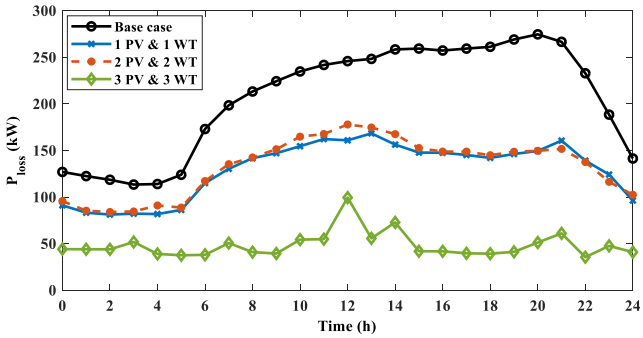

Fig. 6. Hourly active power losses by installing a combined of one PV unit and one wind unit, two PV units and two wind units, and three PV units and three wind units.

proposed approach and the values of the corresponding annual energy losses and average tie-line power are given in Table I. Form Figs. 3–5 and Table I, it can be noted that by increasing the number of combined PV&WT, which are allocated in the microgrid, the annual energy losses and the tie-line power between the utility power grid and the microgrid are significantly decreased. Hence, the microgrid will be more autonomous by increase the number of DG units. For instance, the annual energy loss reductions compared to the base case are 38%, 36.5%, and 77% in the case of allocation a combined of one PV unit and one wind unit, two PV units and two wind units, and three PV units and three wind units, respectively. On the other hand, the tie-line power values are reduced by 80%, 84%, and 90% compared to the base case for a combined of one PV unit and one wind unit, two PV units and two wind units, and three PV units and three wind units, respectively.

The hourly active power losses and tie-line power between the utility power grid and the microgrid are shown in Fig. 6 and Fig. 7, respectively. Compared to the base case, the hourly active power losses and tie-line power are significantly reduced by optimally installing PV and WT units in the microgrid. However, installing a combination of three PV units and three wind units gives better results than installing a combination of one PV unit and one wind unit and two PV units and two wind units. The optimal reactive powers injected/absorbed by the interfacing inverters of PV unis and WT units are illustrated in Fig. 8. In this figure, the positive values mean that the inverters inject the reactive powers, while the negative values indicate that the interfacing inverters absorb the reactive powers. These

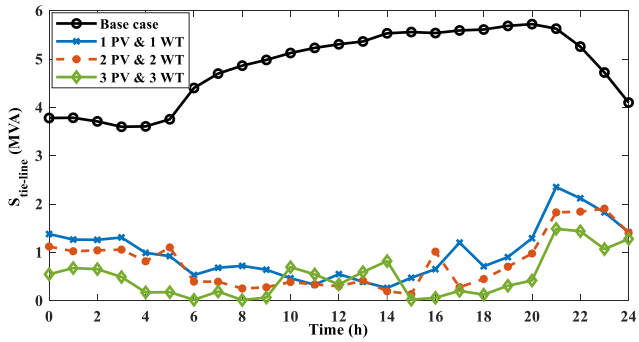

Fig. 7. Hourly tie-line power between the utility power grid and the microgrid by installing a combined of one PV unit and one wind unit, two PV units and two wind units, and three PV units and three wind units.

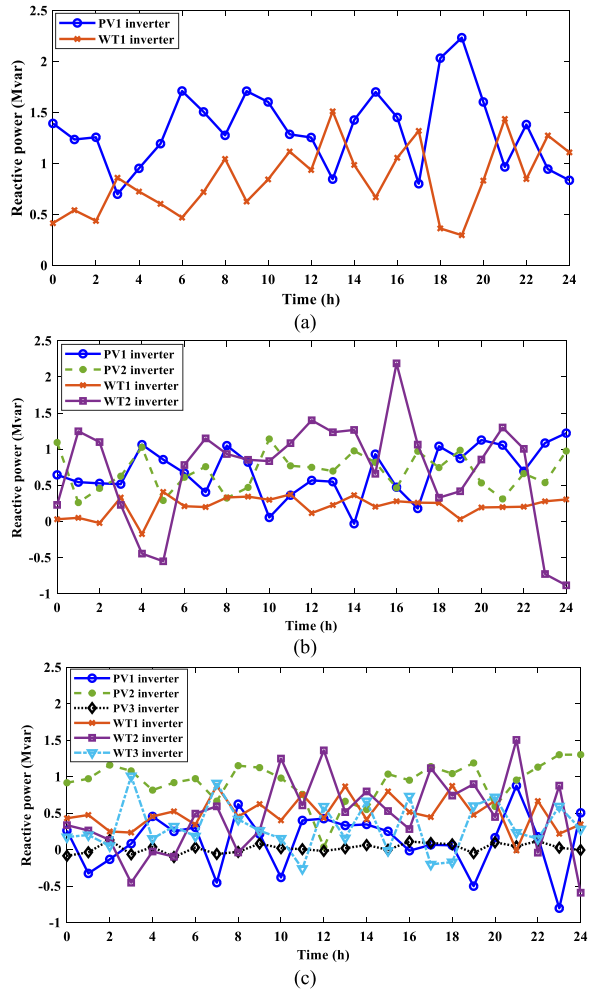

Fig. 8. Hourly reactive power of the interfacing inverters by installing a combined of, (a) one PV unit and one wind unit, (b) two PV units and two wind units, (c) three PV units and three wind units.

optimized reactive powers of DG inverters greatly contribute to minimizing Objectives 1 and 2.

Regarding the charging/discharging power of the PEVs, Fig. 9 shows the charging and discharging power of the four different parking lots in the microgrid. To avoid results reptation, only the charging/discharging powers of the parking lots in the case of

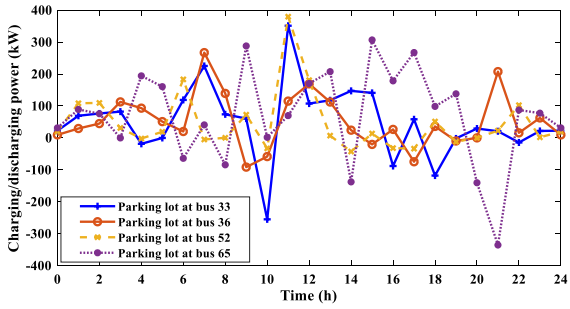

Fig. 9. Hourly charging/discharging power of the PEVs in the case of installing a combined of three PV units and three wind units.

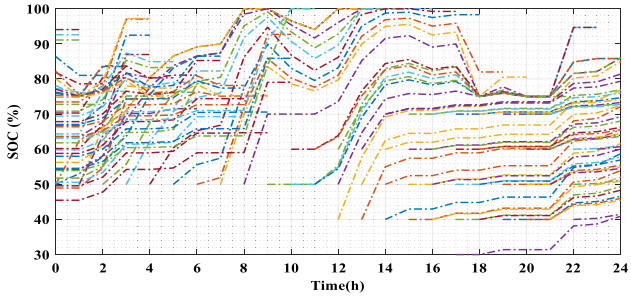

Fig. 10. SOC of the PEVs at bus 36.

TABLE II
OBTAINED SOLUTIONS BY MOPSO AND MOEAD

Item	MOPSO 3PV & 3WT			MOEAD 3PV & 3WT		
PV locations	50	59	66	47	60	69
WT locations	17	32	42	3	30	37
PV sizes (MW)	0.14	1.67	0.10	0.74	0.82	0.44
WT sizes (MW)	2.34	0.38	1.73	1.95	1.35	1.62
Annual energy loss (MWh)	467			661		
Annual energy loss reduction (%)	74.80			64.40		
Average tie-line power (MVA)	0.60			0.43		
Reduction of tie-line power (%)	87.60			91		

TABLE III
OBTAINED SOLUTIONS FOR ALLOCATION 3PV AND 3WT UNITS WITHOUT CONSIDERING THE REACTIVE POWER CAPABILITY

Item	3PV & 3WT		
PV locations	49	61	69
WT locations	9	33	43
PV sizes (MW)	1.57	0.27	0.51
WT sizes (MW)	0.75	1.23	2.30
Annual energy loss (MWh)	710		
Annual energy loss reduction (%)	61.00		
Average tie-line power (MVA)	2.50		
Reduction of tie-line power (%)	48.00		

installing a combined of three PV units and three wind units are shown here. It is worth mentioning that the PEVs that arrive at the end of the previous day have been considered, where they would continue charging at the beginning of the next day. The positive powers indicate that the PEVs are charging from the microgrid while the negative powers indicate that they are discharging to the microgrid. To ensure that the PEVs have enough energy at the parting time for daily mileages, the PEV cannot be employed for V2G if its SOC less than 75%. Fig. 10 depicts the SOC of the PEVs at the parking lot connected to bus 36. It is noticed that the PEVs can charge and discharge to the system (i.e., the SOC are increasing and decreasing) while the SOC of all PEVs at parting time is high enough for daily driving. Regarding the SOC of the PEVs at the other parking lots, they follow the same trend of the displayed figure.

To demonstrate effectiveness of the MOALO, it is compared with two other optimizers: 1) multiobjective particle swarm optimization (MOPSO) [49] and 2) multiobjective evolutionary algorithm based on decomposition (MOEAD) [50] in the case of three PV and three WT units. As noticed from Table II, MOALO can achieve relatively better loss reduction and tie-line power compared to MOPSO and MOEAD. This improvement can be justified by the efficient searching mechanism of MOALO, which can yield the global optimal solutions of PV and WT locations and sizes.

C. Effect of the Inverter Reactive Power

In this part, the effect of the reactive power injected/absorbed by the interfacing inverters on the energy loss and tie-line power in the microgrid is studied. For this purpose, the PV units and WT units are optimally allocated in the microgrid. At the same time, the reactive power capability of the interfacing inverters is disabled, i.e., the interfacing inverters work at unity power factor. Table III shows the results of allocating a combined of three PV units and three WT units without considering the reactive power capability of the interfacing inverters. By comparing Table III with Table I (the case of 3PV and 3WT allocation), the optimal locations and sizes of PV and WT units are changed. For instance, the total size of the PV units is decreased from 2.46 MW to 2.35 MW, and the total size of the WT units is reduced from 4.41 MW to 4.28 MW. On the other hand, the annual energy loss reduction is decreased from 77% to 61%, and the reduction in the tie-line power is reduced from 90% to 48%. This implies that enabling the reactive power capability of the interfacing inverters of the RES has a positive effect on increasing the hosting capacity of RES in the microgrid. Furthermore, it has a significant impact on energy loss reduction and tie-line power reduction.

D. Effect of the OLTC

In this section, the effect of transformer taps at the point of common coupling (PCC) between the utility power grid and microgrid is investigated. Table IV illustrates the results of installing a combined of three PV units and three WT units considering the OLTC at PCC as a control variable. Compared to Table I, the annual energy losses are reduced to only 303 MW compared to 426 in Table I, and the average tie-line power is reduced to only 0.43 MVA compared to 0.5 MVA. The optimal locations of PV units and WT units are different from those in Table I, while the total size of the PV units and WT units are almost the same in which they are 2.44 and 4.43 MW, respectively. This means that employing the OLTC has an evident impact on the microgrid operation and increases the microgrid autonomy. The hourly injected/absorbed reactive power by the interfacing

TABLE IV
OBTAINED SOLUTIONS FOR ALLOCATION 3PV AND 3WT UNITS CONSIDERING THE OLTC

Item	3PV & 3WT		
PV locations	50	61	67
WT locations	6	32	40
PV sizes (MW)	0.69	1.13	0.62
WT sizes (MW)	0.69	2.44	1.30
Annual energy loss (MWh)	303		
Annual energy loss reduction (%)	84.00		
Average tie-line power (MVA)	0.43		
Reduction of tie-line power (%)	91.00		
Number of tap movements	14.00		

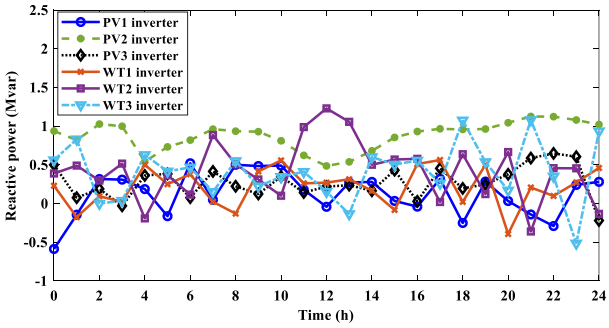

Fig. 11. Hourly reactive power of the interfacing inverters by installing a combined of three PV units and three wind units considering OLTC.

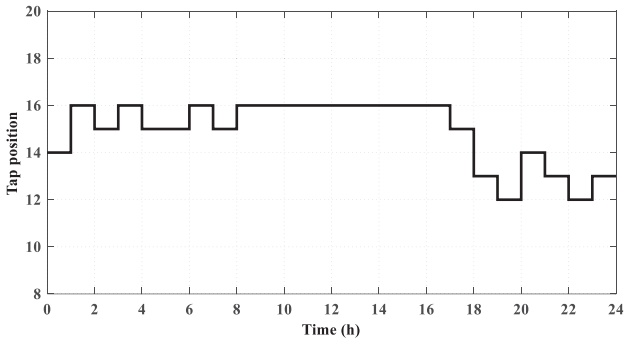

Fig. 12. Optimal tap movements of the OLTC.

inverters and the optimal movements of the OLTC are shown in Fig. 11 and Fig. 12, respectively. It is manifest from Fig. 12 that the OLTC is moved 14 times during the day. It is worth mentioning that the positions of OLTC are decreased by the end of the day to keep the voltages within limits. This because the cumulative number of the PEVs, which can be employed for V2G is increased by the end of the day. Therefore, the amount of active power that can be injected to the microgrid is high.

E. Impact of the PEV Penetration

Here, the impact of the PEV penetration on the allocation problem is investigated. To do so, the capacity of each parking lot is doubled, i.e., each parking lot can accommodate 120 PEVs instead of 60 PEVs. The optimal solutions obtained by applying the proposed approach are given in Table V. From this table, we can note that the increase of the capacity of the charging

TABLE V
OBTAINED SOLUTIONS FOR ALLOCATION 3PV AND 3WT UNITS WITH DOUBLING THE CAPACITY OF THE CHARGING STATIONS

TABLE V OBTAINED SOLUTIONS FOR ALLOCATION 3PV& 3WT UNITS WITH DOUBLING THE CAPACITY OF THE CHARGING STATIONS			
Item	3PV & 3WT		
PV locations	50	61	69
WT locations	7	34	44
PV sizes (MW)	0.24	1.34	1.00
WT sizes (MW)	1.97	0.63	1.34
Annual energy loss (MWh)	254		
Annual energy loss reduction (%)	86.00		
Average tie-line power (MVA)	0.43		
Reduction of tie-line power (%)	91.00		

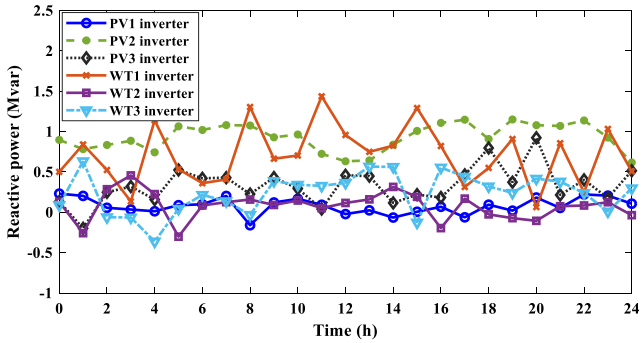

Fig. 13. Hourly reactive power of the interfacing inverters by installing a combined of three PV units and three wind units with doubling the capacity of the charging stations.

stations has an obvious positive impact on energy loss and tie-line reductions. The results given in Table V are better than those given in Tables I and III in terms of annual energy loss reduction and reduction of tie-line power. This implies that by employing the V2G technology of the PEVs, the microgrid can accommodate a high penetration of PEVs with minimum annual energy losses and minimum tie-line power. The hourly reactive power injected/absorbed by the interfacing inverters is depicted in Fig. 13.

F. Discussions

This section compares the different strategies, which are discussed in Sections VI-B, VI-C, VI-D, and VI-E in terms of the total capacity of PV units, the total capacity of WT units, annual energy loss reduction, and reduction of tie-line power (in the case of installing a combined of three PV units and three WT units). Therefore, the different strategies are denoted by Strategy B, Strategy C, Strategy D, and Strategy E. Fig. 14 compares the total sizes of PV units and WT units for different strategies. From this figure, the minimum and maximum PV sizes are 2.35 and 2.56 MW by applying Strategy C and Strategy E, respectively. On the other hand, the minimum and maximum WT sizes are 3.94 and 4.43 MW by using Strategy E and Strategy D, respectively. Furthermore, the annual energy loss reduction and the reduction of tie-line power compared to the base case are shown and compared in Fig. 15. For this figure, the higher reduction in the annual energy loss is achieved by applying Strategy E (i.e., 86%). In comparison, the higher reduction in

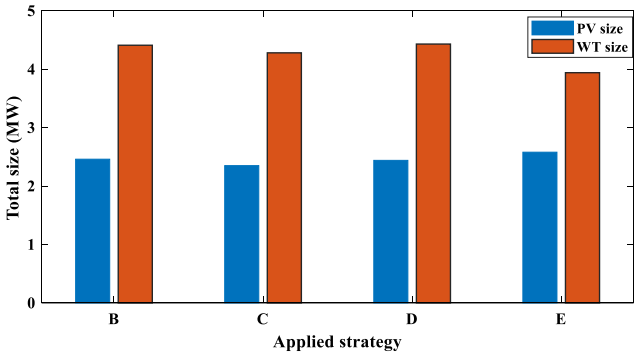

Fig. 14. Total sizes of PV units and WT units by different strategies.

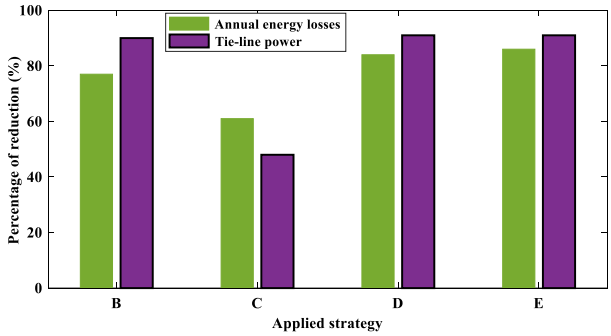

Fig. 15. Annual energy loss reduction and the reduction of tie-line power compared to the base case.

the tie-line power is achieved in Strategy D and Strategy E (i.e., 91%). Therefore, Strategy E is highly recommended to optimize PV and WT generation systems for autonomous microgrids with PEV-parking lots.

VII. Conclusion

In this article, an approach has been proposed to calculate the optimal locations and sizes of PV and WT units in microgrids, considering PEV-parking lots. The merits of the proposed approach are the consideration of the uncertainty of generation profiles of PV units, WT units, loads, and the DSTATCOM feature of PV and WT inverters. Besides, the feasible conditions of PEVs are incorporated in the RES planning model, including 1) initial and preset conditions of their SOC; 2) arriving and departing times; and 3) various controlled/uncontrolled charging schemes. Another vital contribution is to propose a bilevel MOALO solver that accurately solves the planning model. The bilevel MOALO solver involves upper-level and lower-level optimization, which optimize the decision variables of renewable energy sources and PEV, respectively. Both energy losses and energy from the main grid are considered as subobjectives to be minimized by the bilevel MOALO solver. Comprehensive simulations and study cases have been performed to evaluate the effectiveness of the proposed planning approach of RES, considering PEVs. The efficacy of the proposed approach for simultaneously planning PV and WT units and managing PEV for autonomous microgrids.

References

[1] X. Wang, Z. Li, M. Shahidehpour, and C. Jiang, "Robust line hardening strategies for improving the resilience of distribution systems with variable renewable resources," *IEEE Trans. Sustain. Energy*, vol. 10, no. 1, pp. 386–395, Jan. 2019.

[2] N. Liu, J. Wang, and L. Wang, "Hybrid energy sharing for multiple microgrids in an integrated heat-electricity energy system," *IEEE Trans. Sustain. Energy*, vol. 10, no. 3, pp. 1139–1151, Jul. 2019.

[3] J. D. Lara, D. E. Olivares, and C. A. Cañizares, "Robust energy management of isolated microgrids," *IEEE Syst. J.*, vol. 13, no. 1, pp. 680–691, Mar. 2019.

[4] Y. Du, J. Wu, S. Li, C. Long, and S. Onori, "Coordinated energy dispatch of autonomous microgrids with distributed MPC optimization," *IEEE Trans. Ind. Inform.*, vol. 15, no. 9, pp. 5289–5298, Feb. 2019.

[5] J. Ahmad, M. Tahir, and S. K. Mazumder, "Dynamic economic dispatch and transient control of distributed generators in a microgrid," *IEEE Syst. J.*, vol. 13, no. 1, pp. 802–812, Mar. 2019.

[6] D. Xu *et al.*, "Integrated modelling and enhanced utilization of power-to-ammonia for high renewable penetrated multi-energy systems," *IEEE Trans. Power Syst.*, vol. 35, no. 6, pp. 4769–4780, Nov. 2020.

[7] F. D. Kanellos, "Optimal scheduling and real-time operation of distribution networks with high penetration of plug-in electric vehicles," *IEEE Syst. J.*, to be published, doi: 10.1109/JSYST.2020.3006002.

[8] A. Ali, K. Mahmoud, and M. Lehtonen, "Multi-objective photovoltaic sizing with diverse inverter control schemes in distribution systems hosting EVs," *IEEE Trans. Ind. Inform.*, vol. 17, no. 9, Sep. 2021, doi: 10.1109/TII.2020.3039246.

[9] J. Tabatabaei, M. S. Moghaddam, and J. M. Baigi, "Rearrangement of Electrical Distribution Networks With Optimal Coordination of Grid-Connected Hybrid Electric Vehicles and Wind Power Generation Sources," in *IEEE Access*, vol. 8, pp. 219513-219524, 2020, doi: 10.1109/ACCESS.2020.3042763.

[10] European Automobile Manufacturers Association, "A review of battery technologies for automotive applications," Brussels, Belgium, 2014.

[11] C. H. Dharmakeerthi, N. Mithulananthan, and T. K. Saha, "A comprehensive planning framework for electric vehicle charging infrastructure deployment in the power grid with enhanced voltage stability," *Int. Trans. Electr. Energy Syst.*, vol. 25, no. 6, pp. 1022–1040, Jun. 2015.

[12] R. D'hulst, F. De Ridder, B. Claessens, L. Knapen, and D. Janssens, "Decentralized coordinated charging of electric vehicles considering locational and temporal flexibility," *Int. Trans. Electr. Energy Syst.*, vol. 25, no. 10, pp. 2562–2575, Oct. 2015.

[13] S. Xu, H. Pourbabak, and W. Su, "Distributed cooperative control for economic operation of multiple plug-in electric vehicle parking decks," *Int. Trans. Electr. Energy Syst.*, vol. 27, 2017, Art. no. e2348.

[14] N. G. Paterakis and M. Gibescu, "A methodology to generate power profiles of electric vehicle parking lots under different operational strategies," *Appl. Energy*, vol. 173, pp. 111–123, Jul. 2016.

[15] N. Neyestani, M. Y. Damavandi, M. Shafie-Khah, J. Contreras, and J. P. S. Catalao, "Allocation of plug-in vehicles' parking lots in distribution systems considering network-constrained objectives," *IEEE Trans. Power Syst.*, vol. 30, no. 5, pp. 2643–2656, Sep. 2015.

[16] N. Jabalameli and A. Ghosh, "Online centralized coordination of charging and phase switching of PEVs in unbalanced LV networks with high PV penetrations," *IEEE Syst. J.*, vol. 15, no. 1, Mar. 2021, doi: 10.1109/JSYST.2020.3000504.

[17] Y. M. Atwa, E. F. El-Saadany, M. M. A. Salama, and R. Seethapathy, "Optimal renewable resources mix for distribution system energy loss minimization," *IEEE Trans. Power Syst.*, vol. 25, no. 1, pp. 360–370, Feb. 2010.

[18] D. Q. Hung and N. Mithulananthan, "Multiple distributed generator placement in primary distribution networks for loss reduction," *IEEE Trans. Ind. Electron.*, vol. 60, no. 4, pp. 1700–1708, Apr. 2013.

[19] M. Vatani, G. B. Gharehpetian, M. J. Sanjari, and D. Solati Alkaran, "Multiple distributed generation units allocation in distribution network for loss reduction based on a combination of analytical and genetic algorithm methods," *IET Gener. Transmiss. Distrib.*, vol. 10, no. 1, pp. 66–72, Jan. 2016.

[20] K. Mahmoud, N. Yorino, and A. Ahmed, "Optimal distributed generation allocation in distribution systems for loss minimization," *IEEE Trans. Power Syst.*, vol. 31, no. 2, pp. 960–969, Mar. 2016.

[21] M. Kumar and B. Tyagi, "An optimal multivariable constrained nonlinear (MVCNL) stochastic microgrid planning and operation problem with

renewable penetration," *IEEE Syst. J.*, vol. 14, no. 3, pp. 4143–4154, Sep. 2020.
[22] U. Akram, M. Khalid, and S. Shafiq, "Optimal sizing of a wind/solar/battery hybrid grid-connected microgrid system," *IET Renewable Power Gener.*, vol. 12, no. 1, pp. 72–80, Jan. 2018.
[23] X. Wu, X. Hu, Y. Teng, S. Qian, and R. Cheng, "Optimal integration of a hybrid solar-battery power source into smart home nanogrid with plug-in electric vehicle," *J. Power Sources*, vol. 363, pp. 277–283, Sep. 2017.
[24] V. Vahidinasab, "Optimal distributed energy resources planning in a competitive electricity market: Multiobjective optimization and probabilistic design," *Renewable Energy*, vol. 66, pp. 354–363, Jun. 2014.
[25] A. Ali, K. Mahmoud, and M. Lehtonen, "Maximizing hosting capacity of uncertain photovoltaics by coordinated management of OLTC, VAr sources and stochastic EVs," *Int. J. Electr. Power Energy Syst.*, vol. 127, May 2021, Art. no. 106627.
[26] A. Ali, K. Mahmoud, and M. Lehtonen, "Enhancing hosting capacity of intermittent wind turbine systems using bi-level optimisation considering OLTC and electric vehicle charging stations," *IET Renewable Power Gener.*, vol. 14, no. 17, pp. 3558–3567, Dec. 2020.
[27] H. M. H. Farh, A. M. Al-Shaalan, A. M. Eltamaly, and A. A. Al-Shamma'A, "A novel crow search algorithm auto-drive PSO for optimal allocation and sizing of renewable distributed generation," *IEEE Access*, vol. 8, pp. 27807–27820, 2020.
[28] B. R. Pereira, G. R. M. Martins da Costa, J. Contreras, and J. R. S. Mantovani, "Optimal distributed generation and reactive power allocation in electrical distribution systems," *IEEE Trans. Sustain. Energy*, vol. 7, no. 3, pp. 975–984, Jul. 2016.
[29] S. Ganguly and D. Samajpati, "Distributed generation allocation on radial distribution networks under uncertainties of load and generation using genetic algorithm," *IEEE Trans. Sustain. Energy*, vol. 6, no. 3, pp. 688–697, Jul. 2015.
[30] A. Eid, S. Kamel, A. Korashy, and T. Khurshaid, "An enhanced artificial ecosystem-based optimization for optimal allocation of multiple distributed generations," *IEEE Access*, vol. 8, pp. 178493–178513, 2020.
[31] J. Mitra, M. R. Vallem, and C. Singh, "Optimal deployment of distributed generation using a reliability criterion," *IEEE Trans. Ind. Appl.*, vol. 52, no. 3, pp. 1989–1997, May 2016.
[32] H. Bagheri Tolabi, M. H. Ali, and M. Rizwan, "Simultaneous reconfiguration, optimal placement of DSTATCOM, and photovoltaic array in a distribution system based on fuzzy-ACO approach," *IEEE Trans. Sustain. Energy*, vol. 6, no. 1, pp. 210–218, Jan. 2015.
[33] S. U. Jeon, J. Noh, S. Kang, and J.-W. Park, "Practical power management of PV/ESS integrated system," *IEEE Access*, vol. 8, pp. 189775–189785, 2020.
[34] K. Seddig, P. Jochem, and W. Fichtner, "Integrating renewable energy sources by electric vehicle fleets under uncertainty," *Energy*, vol. 141, pp. 2145–2153, Dec. 2017.
[35] K. Qian, C. Zhou, M. Allan, and Y. Yuan, "Modeling of load demand due to EV battery charging in distribution systems," *IEEE Trans. Power Syst.*, vol. 26, no. 2, pp. 802–810, May 2011.
[36] A. Ali, D. Raisz, K. Mahmoud, and M. Lehtonen, "Optimal placement and sizing of uncertain PVs considering stochastic nature of PEVs," *IEEE Trans. Sustain. Energy*, vol. 11, no. 3, pp. 1647–1656, Jul. 2020.
[37] A. Ali, K. Mahmoud, D. Raisz, and M. Lehtonen, "Optimal allocation of inverter-based WTGS complying with their DSTATCOM functionality and PEV requirements," *IEEE Trans. Veh. Technol.*, vol. 69, no. 5, pp. 4763–4772, May 2020.
[38] A. Soroudi, "Possibilistic-scenario model for DG impact assessment on distribution networks in an uncertain environment," *IEEE Trans. Power Syst.*, vol. 27, no. 3, pp. 1283–1293, Aug. 2012.
[39] M. A. Akbari *et al.*, "New metrics for evaluating technical benefits and risks of DGs increasing penetration," *IEEE Trans. Smart Grid*, vol. 8, no. 6, pp. 2890–2902, Nov. 2017.
[40] A. Ali, K. Mahmoud, D. Raisz, and M. Lehtonen, "Probabilistic approach for hosting high PV penetration in distribution systems via optimal oversized inverter with watt-var functions," *IEEE Syst. J.*, vol. 15, no. 1, pp. 684–693, Apr. 2020.
[41] R. H. A. Zubo, G. Mokryani, and R. Abd-Alhameed, "Optimal operation of distribution networks with high penetration of wind and solar power within a joint active and reactive distribution market environment," *Appl. Energy*, vol. 220, pp. 713–722, 2018.
[42] S. Mirjalili, P. Jangir, and S. Saremi, "Multi-objective ant lion optimizer: A multi-objective optimization algorithm for solving engineering problems," *Appl. Intell.*, vol. 46, no. 1, pp. 79–95, Jan. 2017.
[43] S. R. Ghatak, S. Sannigrahi, and P. Acharjee, "Multi-objective approach for strategic incorporation of solar energy source, battery storage system, and DSTATCOM in a smart grid environment," *IEEE Syst. J.*, vol. 13, no. 3, pp. 3038–3049, Sep. 2019.
[44] M. E. Baran and F. F. Wu, "Network reconfiguration in distribution systems for loss reduction and load balancing," *IEEE Trans. Power Del.*, vol. 4, no. 2, pp. 1401–1407, Apr. 1989.
[45] X. Wu, X. Hu, S. Moura, X. Yin, and V. Pickert, "Stochastic control of smart home energy management with plug-in electric vehicle battery energy storage and photovoltaic array," *J. Power Sources*, vol. 333, pp. 203–212, 2016.
[46] A. Andreas and T. Stoffel, Nevada Power: Clark Station; Las Vegas, Nevada (Data); NREL Report No. DA-5500-56508, 2006, doi: 10.5439/1052547.
[47] "Historical climate data - Climate - environment and climate change canada," 2019. Accessed: Aug. 28, 2019. [Online]. Available: http://climate.weather.gc.ca/
[48] "European network of transmission system operators for electricity," 2019. Accessed: Aug. 28, 2019. [Online]. Available: https://www.entsoe.eu/
[49] M. Z. bin Mohd Zain, J. Kanesan, J. H. Chuah, S. Dhanapal, and G. Kendall, "A multi-objective particle swarm optimization algorithm based on dynamic boundary search for constrained optimization," *Appl. Soft Comput. J.*, vol. 70, pp. 680–700, Sep. 2018.
[50] Q. Zhang and H. Li, "MOEA/D: A multiobjective evolutionary algorithm based on decomposition," *IEEE Trans. Evol. Comput.*, vol. 11, no. 6, pp. 712–731, Dec. 2007.

Abdelfatah Ali received the B.Sc. and M.Sc. degrees in electric power engineering from Aswan University, Aswan, Egypt, in 2009 and 2013, respectively, and the Ph.D. degree in electric power engineering from the Doctoral School of Electrical Engineering, Budapest University of Technology and Economics, Budapest, Hungary, in 2020.

Since 2010, he has been an Assistant Lecturer with the Faculty of Engineering, South Valley University (SVU), Qena, Egypt. He is currently working as an Assistant Professor with South Valley University. His research interests include power systems, renewable energy sources, distributed generation, electric vehicles, and optimization.

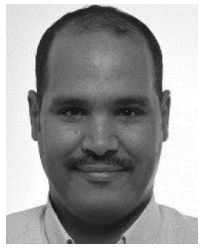

Karar Mahmoud received the B.Sc. and M.Sc. degrees in electrical engineering from Aswan University, Aswan, Egypt, in 2008 and 2012, respectively, and the Ph.D. degree in electrical engineering from the Electric Power and Energy System Laboratory (EPESL), Graduate School of Engineering, Hiroshima University, Hiroshima, Japan, in 2016.

Since 2010, he has been with Aswan University, where he is currently working as an Associate Professor with the Department of Electrical Engineering, Faculty of Engineering, Aswan University. He is also a Postdoctoral Researcher with the Group of Prof. M. Lehtonen, School of Electrical Engineering, Aalto University, Finland. He has authored or coauthored several publications in top-ranked journals, including IEEE journals, international conferences, and book chapters. His research interests include power systems, renewable energies, smart grids, distributed generation, optimization, applied machine learning, the IoT, Industry 4.0, and high voltage.

Dr. Mahmoud has also been a Topic Editor in the *Sensors* journal since 2021.

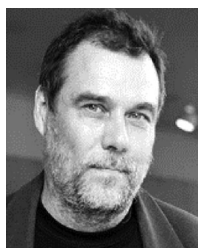

Matti Lehtonen received the master's and Licentiate degrees in electrical engineering from the Helsinki University of Technology, Espoo, Finland, in 1984 and 1989, respectively, and the Doctor of Technology degree in electrical engineering from Tampere University of Technology, Tampere, Finland, in 1992.

He was with VTT Energy, Espoo, Finland, from 1987 to 2003, and since 1999 has been a Full Professor and Head of power systems and high voltage engineering group's with Aalto University, Espoo, Finland. His research interests include power system planning and assets management, power system protection including earth fault problems, harmonic-related issues, high-voltage systems, power cable insulation, and polymer nanocomposites.

Prof. Lehtonen is an Associate Editor for *Electric Power Systems Research* and *IET Generation, Transmission and Distribution*.